Supporting Information

Impact of mutations on the conformational transition from α-helix to β-sheet structures in Arctic-type $A\beta_{40}$: Insights from molecular dynamics simulations

Rajneet Kaur Saini[¶], Suniba Shuaib[¶‡], Deepti Goyal[¶*] and Bhupesh Goyal[§*]

[¶]Department of Chemistry, Faculty of Basic and Applied Sciences,
Sri Guru Granth Sahib World University, Fatehgarh Sahib–140406, Punjab, India
[§]School of Chemistry & Biochemistry, Thapar Institute of Engineering & Technology,
Patiala–147004, Punjab, India

*Corresponding authors

Email: deeptig@iitbombay.org; bhupesh@thapar.edu

Current address:
[‡]Biotech Analyst, Biopharmaceutical Services
SGS Canada Inc.
6490 Vipond Drive, Mississauga, ON, L5T 1W8

Table of contents

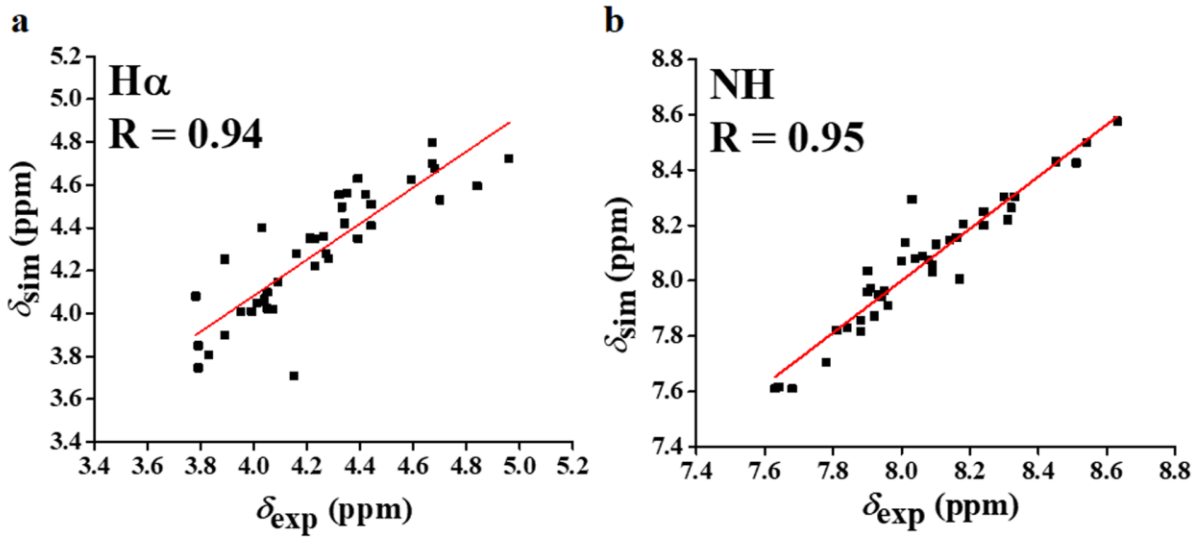

Figure S1. The correlation between simulated and experimental ^{1}H NMR chemical shifts for Hα atoms, and amide protons of [G22]Aβ_{40} residues are shown in panel a, and b, respectively. The unit of chemical shift is ppm and R represent the correlation coefficient.

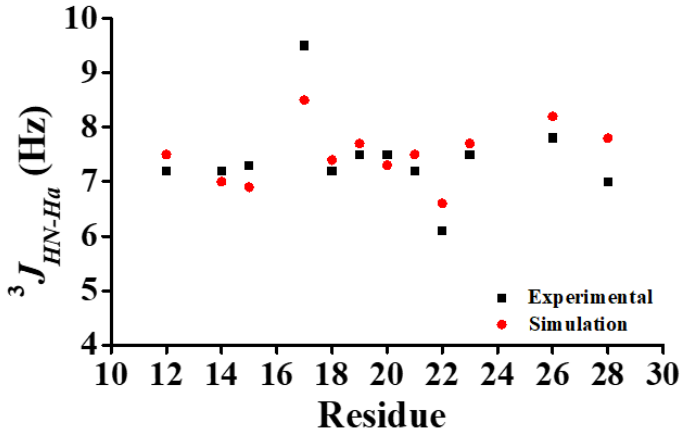

Figure S2. Comparison of simulated $^3J_{HN\text{-}H\alpha}$ coupling constants of [G22]Aβ_{40} residues (red) with experimental measurements published in 2008 (black).

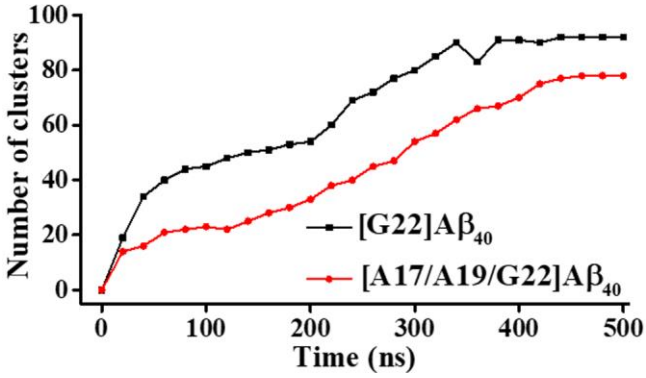

Figure S3. The evolution of clusters for [G22]Aβ_{40} (black) and [A17/A19/G22]Aβ_{40} (red) is shown during simulation. Y–axis represents number of microstates and X–axis represents molecular dynamics simulation time in ns.

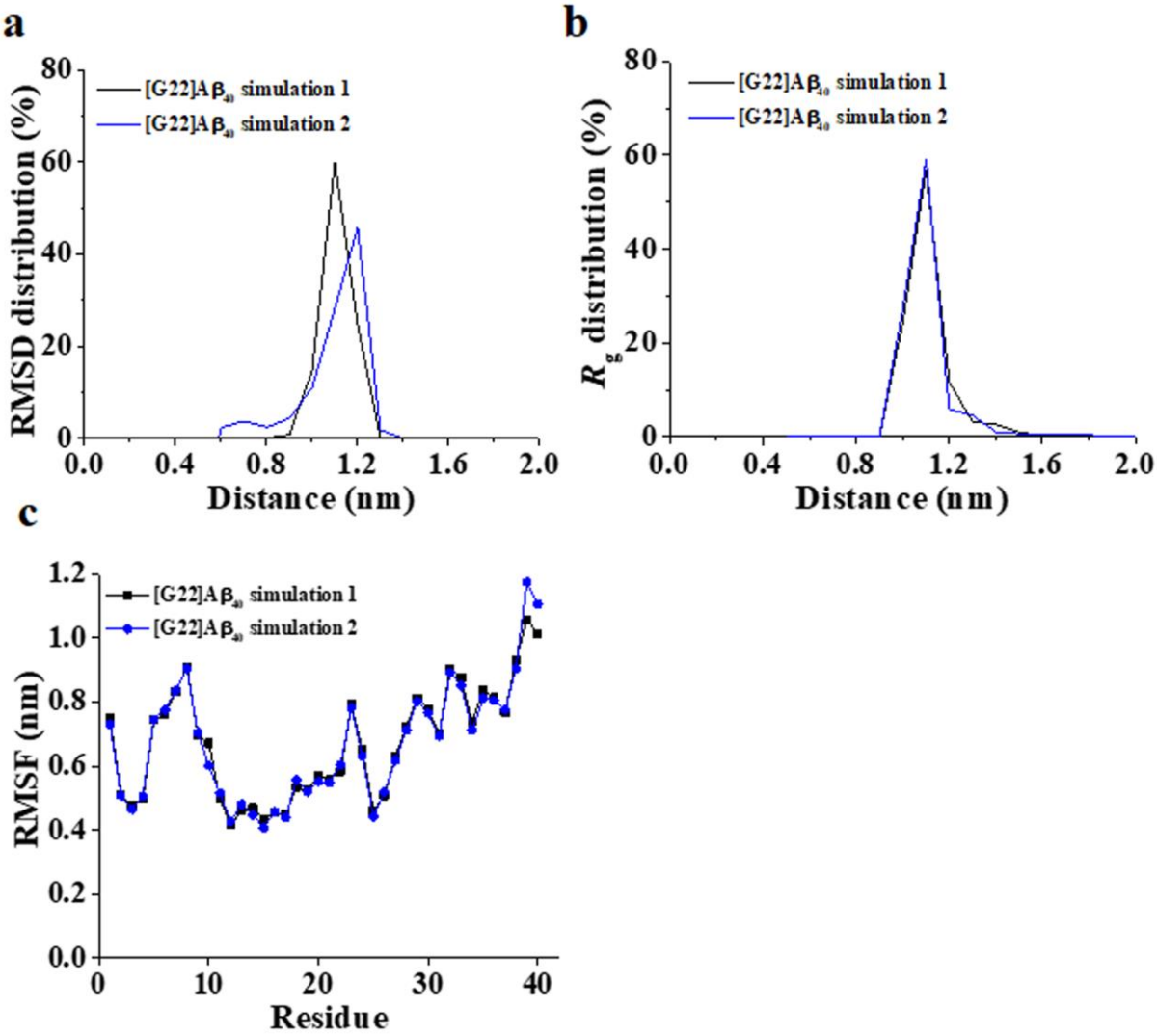

Figure S4. The root-mean-square deviation (RMSD) and radius-of-gyration (R_g) distribution of [G22]Aβ40 for simulations with different initial velocities are shown in panel a, and b, respectively. The root-mean-square fluctuation (RMSF) of each residue in [G22]Aβ40 for simulations with different initial velocities is shown in panel c. The RMSD, R_g and RMSF data for simulation 1 and 2 of [G22]Aβ40 are represented by black and blue, respectively.

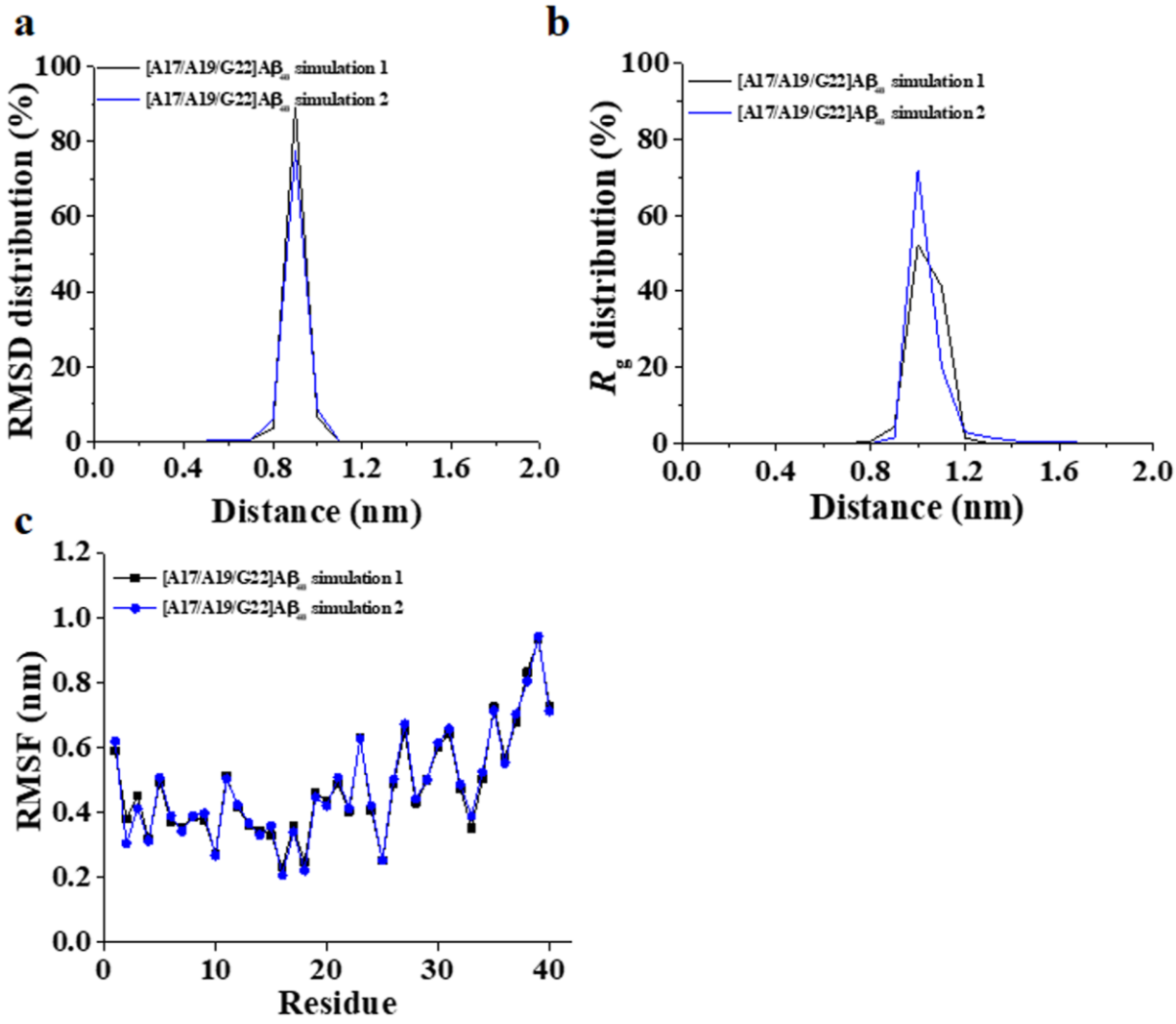

Figure S5. The RMSD and R_g distribution of [A17/A19/G22]Aβ_{40} for simulations with different initial velocities are shown in panel a, and b, respectively. The RMSF of each residue in [A17/A19/G22]Aβ_{40} for simulations with different initial velocities is shown in panel c. The RMSD, R_g and RMSF data for simulation 1 and 2 of [A17/A19/G22]Aβ_{40} are represented by black and blue, respectively.

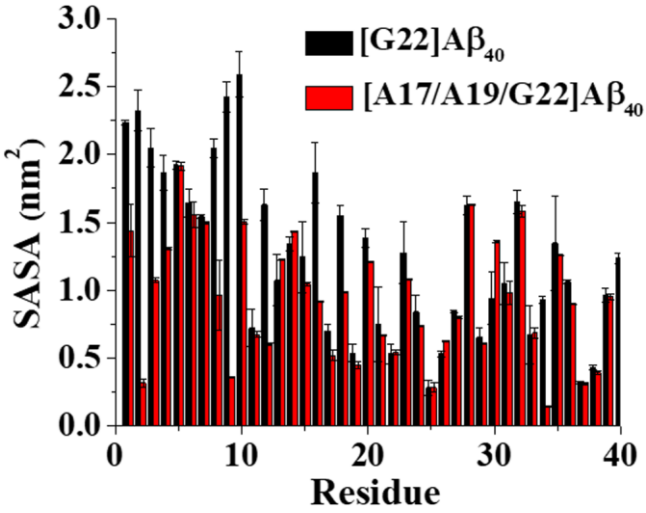

Figure S6. The solvent accessible surface area (SASA) of each residue in [G22]$A\beta_{40}$ and [A17/A19/G22]$A\beta_{40}$.

Table S1. The secondary structure component statistics of [G22]Aβ_{40} and [A17/A19/G22]Aβ_{40} for simulations with different initial velocities. The standard error was evaluated by dividing the simulation data into three non-overlapping blocks.

Model system	helix[a]	β-sheet[b]	turn	coil	bend
[G22]Aβ_{40} (simulation 1)	7 ± 2.25	14 ± 0.88	21 ± 2.60	31 ± 1.15	17 ± 3.00
[G22]Aβ_{40} (simulation 2)	5 ± 2.87	15 ± 1.86	23 ± 2.94	30 ± 1.06	19 ± 2.94
[A17/A19/G22]Aβ_{40} (simulation 1)	13 ± 1.34	7 ± 1.85	17 ± 2.73	27 ± 0.57	26 ± 1.88
[A17/A19/G22]Aβ_{40} (simulation 2)	14 ± 2.77	9 ± 2.54	16 ± 1.17	28 ± 0.95	25 ± 2.35

[a]helix comprises 3_{10}, α–, and π–helix ; [b]β-sheet comprises β-strand and β-bridge